Surface Electrochemistry of CO and H_2/CO Mixtures at Pt(100) Interface: Electrode Kinetics and Interfacial Structures

N. M. Marković,*,† C. A. Lucas,‡ B. N. Grgur,† and P. N. Ross†

Materials Sciences Division, Lawrence Berkeley National Laboratory, University of California, Berkeley, California 94720, and Oliver Lodge Laboratory, Department of Physics, University of Liverpool, Liverpool, L69 7ZE, UK

Received: May 13, 1999; In Final Form: August 24, 1999

The Pt(100)−CO interaction in aqueous electrolytes was examined by using rotating disk methods in combination with in-situ surface X-ray scattering (SXS) measurements. The analysis of the SXS results indicates that the topmost platinum atoms expand away from the second layer by ca. 4% when H_{upd} was completely displaced from Pt(100) by CO to form a saturated layer of CO. Assuming that gas-phase heats of adsorption for CO apply as well to the liquid−solid interface, we estimate that the Gibbs energy change for the displacement of H_{upd} by CO on Pt(100) is close to −90 kJ/mol. A Pt(100)−CO surface normal interlayer spacing of 1.4 ± 0.4 Å was extracted from SXS measurements, suggesting that CO is adsorbed primarily at the 2-fold bridge-bonded sites, or possibly a mixture of bridge and atop sites. In contrast to the Pt(111)−CO system, no structures of CO_{ad} with long-range order were formed on Pt(100). Two different forms of CO_{ad} are formed at the Pt(100)−electrolyte interface: the weakly adsorbed state which is oxidized in the pre-ignition potential region, and the strongly adsorbed state which is oxidized in the ignition potential region. Although the nature of CO_{ad} is different before and after the ignition potential, we proposed that the mechanism for CO oxidation on Pt(100) is the same in both the pre-ignition and ignition potential regions, e.g., adsorbed CO reacts with hydroxyl species (OH_{ad}) through a Langmuir−Hinshelwood type reaction. The kinetics of CO oxidation on Pt(*hkl*) surfaces is found to vary with crystal face. The difference in activity is attributed to the structure-sensitive adsorption of CO, OH_{ad}, and anions from the supporting electrolytes.

1. Introduction

The irreversible adsorption of CO (hereafter denoted as CO_{ad}) on Pt(*hkl*) and its electrooxidative removal has been extensively investigated in both CO-free solution and in solution saturated with gaseous CO (hereafter denoted as CO_b).[1−19] In previous work in this laboratory, electrocatalysis of CO_b oxidation and the interfacial structure of the CO_{ad} adlayer on the Pt(110)-(1 × 1),[17] Pt(110)-(1 × 2),[17] and Pt(111)-(1 × 1)[19] surfaces in 0.5 M H_2SO_4 were examined by using the rotating disk electrode method in combination with in-situ surface X-ray diffraction measurements. In-situ X-ray scattering measurements indicated that in a solution containing CO_b, the Pt(111)-(1 × 1),[19] Pt-(110)-(1 × 2),[17] and Pt(110)-(1 × 1)[17] surface structures are stable in the potential region between 0 and 1.0 V vs the reversible hydrogen electrode (RHE). It is important to note that adsorption of CO_{ad} even to full coverage on the (1 × 2) surface in solution does not induce the (1 × 2) → (1 × 1) transition that is observed in UHV upon adsorption of CO_{ad}.[17] Nominally identical saturation coverages of CO_{ad} are observed on the two surfaces, ca. one monolayer (ML), implying that two CO_{ad} molecules are adsorbed per unit cell of the reconstructed (1 × 2) surface. The (1 × 2) surface is found to have a much higher catalytic activity for the electrooxidation of CO than the (1 × 1) surface. The anodic oxidation of either CO_{ad} or CO_b occurs at a potential 0.3−0.5 V lower on the (1 × 2) surface versus the (1 × 1) surface. For Pt(110)−CO_{ad} systems, we attributed this difference in kinetics to an increased in the surface coverage by oxygen-containing species (hereafter denoted as OH_{ad}), and/or an higher mobility of CO_{ad} on the reconstructed surface compared to the unreconstructed surface.[17] The results for the Pt(111)−CO_{ad} system in 0.5 M H_2SO_4 showed that the saturation surface coverage of CO_{ad} on the Pt-(111) surface is ca.0.75 ML, with the CO_{ad} assuming a compressed p(2 × 2) structure containing 3 CO_{ad} molecules in the unit cell.[19] These studies clearly revealed that the p(2 × 2)-3CO_{ad} structure formed what we called the "weakly adsorbed state" of CO_{ad} (hereafter denoted as $CO_{ad,w}$), which is oxidized at lower overpotentials in a so-called pre-ignition potential region.[19] We found that oxidative removal of a fraction of the $CO_{ad,w}$ state is accompanied by a simultaneous relaxation of the remaining CO_{ad} that produces a new binding state which we characterized as a "strongly adsorbed state" of CO_{ad} (hereafter denoted as $CO_{ad,s}$). $CO_{ad,s}$ is oxidized from the surface in a so-called ignition potential region,[19] where the current rises to the (CO_b) diffusion-limited current. These two states are distinguished primarily by the strength of the CO_{ad}−CO_{ad} repulsive interaction at high coverage rather than by occupation of specific sites.

The present study of the Pt(100)−CO_{ad} system was undertaken to complete our study of the role of the surface structure in the kinetics of oxidative removal of CO_{ad} in acid solutions. To establish the dynamics of formation of "holes" in the CO_{ad} adlayer, we also present experimental data for the electrooxidation of molecular hydrogen (HOR) on the Pt(100) surface which is fully or partially covered by CO_{ad}. We also reported

* Corresponding author. Lawrence Berkeley National Laboratory, Mail Stop 2-100, Berkeley, CA 94720. E-mail: nmmarkovic.lbl.gov.
† Lawrence Berkeley National Laboratory, University of California.
‡ Department of Physics, University of Liverpool.

10.1021/jp991566g CCC: $18.00
Published on Web 10/15/1999

results for the electooxidation of H_2/2% CO mixture under well-defined mass transfer conditions, which highlight differences in kinetics of the HOR with and without the process of readsorption of CO_b. The electrochemical measurements are augmented by in-situ surface X-ray scattering results, which provided an independent (nonelectrochemical) measure of the structure and coverage of CO_{ad} on Pt(100) under dynamic conditions. Finally, the comparison in CO oxidation kinetics between the different platinum single crystals shed considerable light on the importance of defect sites for nucleation of OH_{ad} in the pre-ignition region. These results provide important insight into the reaction mechanism of CO-poisoning of the HOR and contribute to the quest for a CO-tolerant fuel cell anode electrocatalyst.

2. Experimental Section

Most of the experimental details were described previously. Following the flame annealing-hydrogen (or argon) cooling method, the Pt(100) electrode was transferred into the disk configuration of the rotating ring-disk electrode, RRDE. The cleanliness of the transfer and the electrolyte, even under sustained rotation at high rotation rates, was demonstrated in our previous work.[20] For CO_{ad} stripping voltammetry the electrolyte (0.5 M H_2SO_4, Baker *Ultrex*) was saturated with CO_b, and the electrode was immersed into the electrolyte under potential control at five different potentials. Subsequently, the electrode was rotated at 2500 rpm for 5 min to allow for the complete poisoning of the electrode surface with CO before purging CO_b from the solution with argon. After recording CO_{ad} stripping voltammetry, the Pt(100) surface was again poisoned by CO_{ad} at 0.05 V for 10 min, and then the CO was purged from solution with pure H_2. Hydrogen oxidation currents were then recorded potentiodynamically on the Pt(100) surface covered by the CO_{ad} adlayer. For the electrooxidation of a dissolved pure CO gas (denoted hereafter as CO_b) and H_2 (Ar)/CO mixture the electrolyte was equilibrated for 5 min with the respective gas/mixture, while the electrode potential was held at 0.05 V, before potentiodynamic measurements were performed.

In surface X-ray diffraction measurements the X-ray cell was mounted either at the center of a 2 + 2 circle goniometer on beamline ID 10 B at the European Synchrotron Radiation Facility (ESRF), Grenoble, or on a four-circle goniometer on beamline 7-2 at the SSRL. The outer shell of the electrochemical X-ray cell was purged either with nitrogen or with CO. The CO diffused through the thin polypropylene film trapping in the electrolyte, and adsorbed (dynamically) onto the Pt(100) surface while under potential control. For more experimental details see references.[19,21]

The pure gases as well as the CO/Ar and CO/ H_2 mixtures were purchased from Matheson (Matheson purity: 4N CO, 5N Ar, and 6N H_2). All potentials are referred to RHE at room temperature, and current densities are based on the geometric surface area (0.283 cm^2).

3. Results

3.1. Stripping Voltammetry of CO_{ad} and HOR on Pt(100)−CO_{ad}. The base voltammogram of Pt(100) in 0.5 M H_2SO_4 from our laboratory was published previously.[20] The characteristic voltammetric features from an ordered Pt(100) structure in sulfuric acid are the two delineated peaks at 0.4 and 0.3 V, which correspond to the coupled processes of hydrogen adsorption with the bisulfate anion desorption on (100) terrace sites and $n(100) \times (111)$ step sites, respectively.[22] The

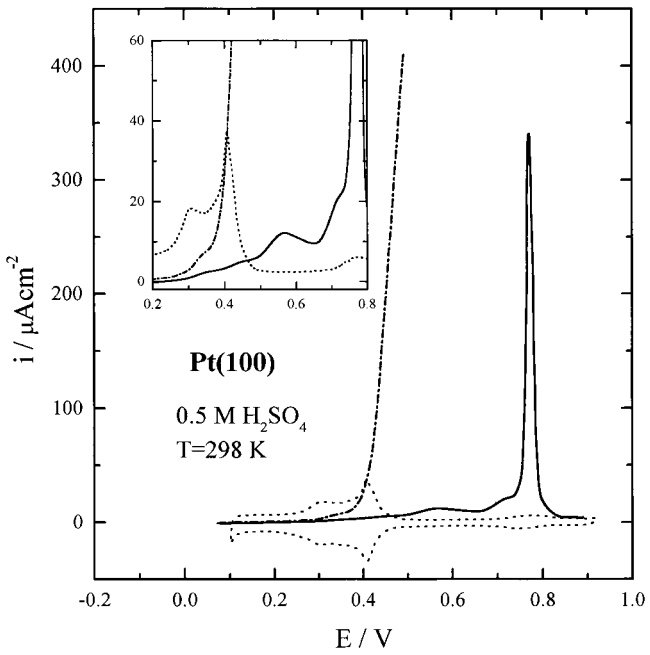

Figure 1. (—) CO stripping voltammetry on the Pt(100) surface in argon-purged solution. CO was adsorbed at the negative potential limit (0.05 V): (- - -) polarization curve for the HOR on the Pt(100) surface which was covered with the preadsorbed CO_{ad} at 0.05 V: (- - -) the first negative sweep after stripping of CO_{ad}. Insert: Magnification of the pre-ignition region for the positive-going sweep. Sweep rate 20 mV/s.

potential region of the H_{upd} is followed first by a reversible adsorption of hydroxyl species (H_2O being the source of OH_{ad}) in the potential range $\approx 0.7 < E < 0.8$ V, and then by an irreversible adsorption of a platinum "oxide" ($E > 0.9$ V). The anodic stripping voltammetry of CO in argon-purged solution along with the polarization curve for the HOR dissolved in the bulk electrolyte are shown in Figure 1. The stripping voltammetry of CO_{ad} shows that, upon sweeping the potential positively from 0.05 V, the onset of oxidation of CO_{ad} in the Ar-purged solution commences at ≈0.3 V, forming what we have previously referred to as a pre-ignition wave over the potential region of ≈0.3−0.7 V.[19] Note that the onset of CO_{ad} oxidation begins at 0.3 V, i.e., it is mirrored with the peak we have assigned to the adsorption/desorption of H_{upd} concomitant to desorption/adsorption of anions *on* the step sites. Closely following our interpretation for CO_{ad} stripping voltammetry on Pt(111),[19] we propose that the pre-ignition potential region is produced by the electrooxidative removal of the $CO_{ad,w}$ state. Above 0.75 V, the CO_{ad} stripping voltammetry is characterized by a sharp peak centered at ≈0.77 V. Again, using our terminology for the state of CO_{ad} which is oxidized in the potential region where the reversible adsorption of OH_{ad} is observed in the base voltammetry, we suggest that the stripping peak is produced by the surface reaction involving interaction between OH_{ad} and $CO_{as,s}$.[19] In this work, the positive potential limit was chosen so as to entirely strip the preadsorbed CO_{ad} from the Pt(100) surface but to avoid irreversible disordering of the surface, e.g. $E < 1.0$ V. Figure 1 confirms that the successive negative-going sweep and the second cycle trace accurately the base voltammetry of a clean Pt(100) surface.

The result for the electrooxidation of gaseous H_2 dissolved in the bulk electrolyte (dotted curve in Figure 1) on the platinum surface completely covered with the CO_{ad} state indicates that while the onset of the HOR is observed at ca. 0.25 V, a sharp increase in kinetics is recorded at ca. 0.4 V. The inset of Figure 1 shows magnification of the pre-ignition potential region. Quite

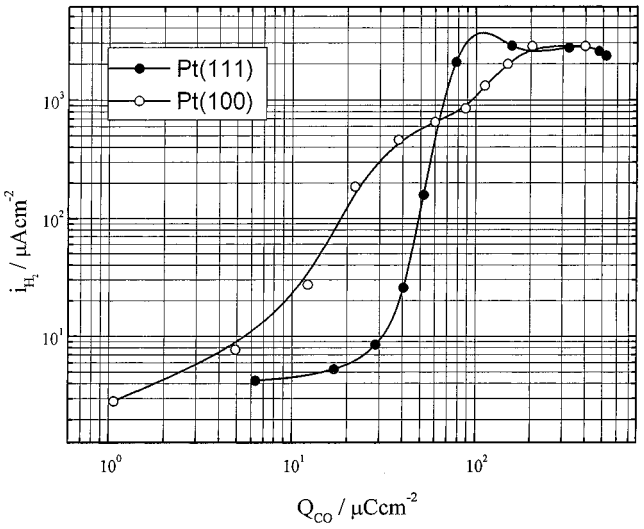

Figure 2. Correlation between the rate of the HOR and the stripping charge for the oxidative removal of CO_{ad} on Pt(100) and Pt(111) surfaces in 0.5 M H_2SO_4.

clearly, the onset of the HER coincides with the potential at which the oxidative removal of $CO_{ad,w}$ is observed in the stripping voltammetry, indicating that H_2 oxidation current occurs *concurrently* with the removal of the $CO_{ad.w}$ state. A diffusion-limiting current for the HOR (not shown) is observed above ca. 0.75 V, corresponding to removal of about 30% of the total amount of CO_{ad} present from adsorption at 0.05 V, see Figure 2. For comparison, a correlation between the rate of the HOR and the stripping charge for the oxidative removal of CO_{ad} on the Pt(111) surface is also shown in Figure 2.

Figure 3 summarizes a set of linear sweep voltammetry curves for the anodic stripping of CO_{ad} preadsorbed at various potentials. Figure 3 also shows the superimposed polarization curves for the HOR (in H_2-saturated solution) on the Pt(100)−CO_{ad} surface. Three main features characterize the effects of CO_{ad} preadsorption potential on the stripping voltammetry. The first is that the pre-ignition wave is observed only if CO_{ad} is preadsorbed between $0.0 < E < 0.45$ V. This suggests that removal of $CO_{ad,w}$ takes place continuously during replacement of CO_b with purging Ar (and/or H_2) through the solution at $E < \approx 0.45$ V. The second is that the major CO_{ad} stripping peak at ≈ 0.75 V becomes sharper if CO_{ad} is preadsorbed at more positive potentials. The third characteristic is that the surface coverage (as indicated by the charge under the stripping peak) of CO_{ad} decreases with increasing adsorption potential, from 410 μC/cm^2 at 0.05 V to 311 μC/cm^2 at 0.4 V. The effects of the preadsorption potential on the HOR, i.e., the linear sweep voltammetry for the solution saturated with H_2, are shown as the dotted curves in Figure 3. Note that the onset of the current from the HOR is shifted positively if CO_{ad} is preadsorbed at more positive potentials, implying that the HOR on CO-covered surfaces are *transient currents observed only simultaneously with CO_{ad} oxidation*. Though many more experiments were conducted, the examples in Figure 3 demonstrate the general pattern of the CO_{ad} stripping voltammetry on Pt(100), which is similar to that on the Pt(111)−CO_{ad} system.[19]

3.2. Electrooxidation of CO_b and H_2/CO Mixtures. Although the stripping voltammetry of CO_{ad} provides valuable information on the surface chemistry of CO_{ad} on Pt(100), only the continuous supply of CO_b to the electrode surface enables true determination of the catalytic activity of Pt(100) for the oxidation of CO_{ad}. Figure 4a shows that oxidation of CO_b begins at a much more positive potentials than that observed in the

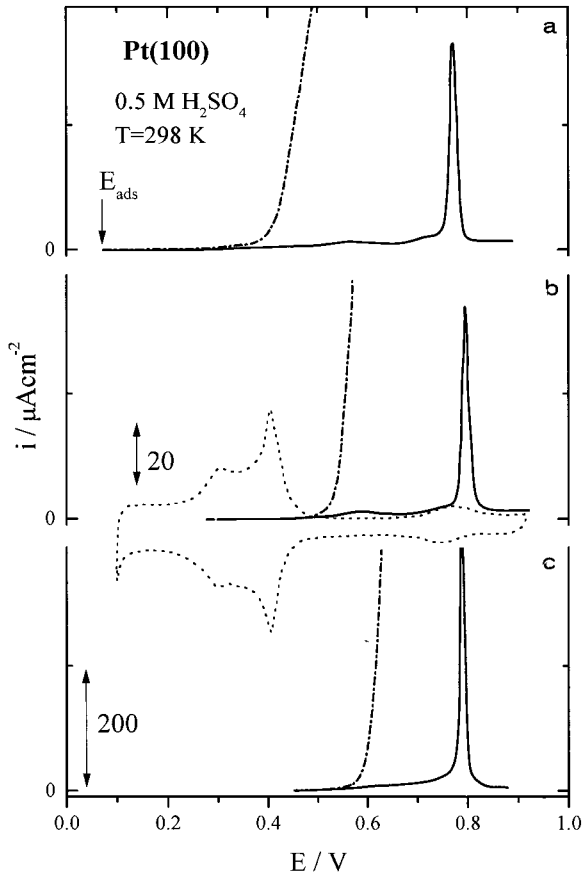

Figure 3. (—) Stripping voltammetry of CO_{ad} which is preadsorbed at different potentials on the Pt(100) surface in argon-purged 0.5 M H_2SO_4 solution: (- - -) polarization curves for the HOR on the Pt(100) surface covered with CO_{ad} which preadsorbed at three different potentials. Sweep rate 20 mV/s.

stripping voltammetry; e.g., the pre-ignition region is followed by the oxidation of CO_b which is observed as a sharp increase in the current at the ignition potential at ca. 0.95 V. The ignition potential region, characterized by a step rise in the oxidation current to the diffusion-limiting current, is concurrent with the oxidation of $CO_{ad,s}$. It is important to note that the pre-ignition region was also observed in the polarization curve for the 2% CO/Ar mixture, Figure 4b. A comparison of these potentiodynamic curves (inset of Figure 4) clearly reveals that a reduced partial pressure of CO produces a *decrease* in the rate of CO_b electrooxidation, consistent with a *positive* reaction order for CO_b oxidation with respect to partial pressure of CO. Recently, a positive reaction order with respect to CO_b partial pressure has also been observed within the pre-ignition region for the electrooxidation of CO_b on polycrystalline Pt electrodes and Pt-(111).[19] If the partial pressure of CO is reduced from 1 to 0.02 by means of a CO/Ar mixture, the "ignition" potential of CO oxidation shifts *negatively* versus pure CO ($\approx$0.18 V in Figure 4), producing a negative reaction order for the oxidation of CO_b on Pt at $E > 0.85$ V. This implies that the reaction order with respect to CO_b can be either positive or negative, depending on the nature of CO_{ad} on the platinum surface and the surface coverage by OH_{ad}. The electrooxidation of the 2% CO/H_2 mixture was measured on Pt(100) using the same potentiodynamic method used with the pure CO and the CO/Ar mixture. Figure 4 shows the polarization curve for oxidation of 2% CO/H_2 on Pt(100). Clearly, the transition from an inactive, i.e., poisoned, surface to a highly active surface occurs in a very narrow potential band, and is clearly related to the ignition of CO_b oxidation at $\approx$0.85 V (in H_2-free solution). In fact, the

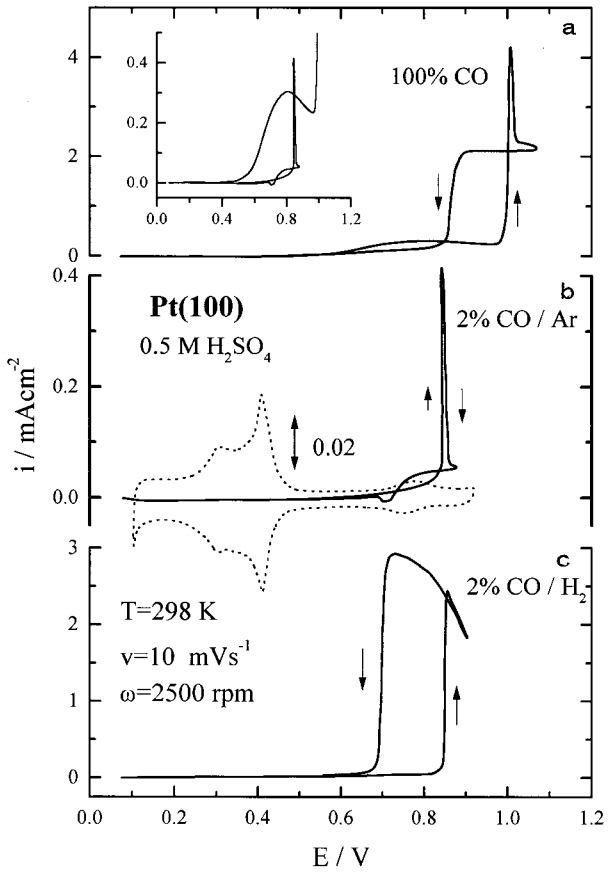

Figure 4. (a) Potentiodynamic CO_b oxidation current densities on Pt-(100) in 0.5 M H_2SO_4 saturated with CO_b. (b) Potentiodynamic CO oxidation current for the 2% CO/Ar mixture on Pt(100). (c) Potentiodynamic HOR current densities on Pt(100) in 0.5 M H_2SO_4 saturated with 2% CO/Ar mixture. Insert: Magnification of the preoxidation region from (a) and (b). Sweep rate 5 mV/s.

steady-state currents in the 0.75−0.8 V region for 2% CO/H_2 are approximately a constant multiple of the oxidation current for 2% CO/Ar, ca. a factor 40.

3.3. X-ray Scattering Measurements. As in the case of Pt-(110)−CO_{ad} and Pt(111)−CO_{ad} systems,[17,19] a precise description of structure at the Pt(100)−CO electrochemical interface, in particular with respect to the surface Pt layer, can be obtained by measuring both the specular and nonspecular crystal truncation rods (CTR). First of all, we should point out that we have never observed the Pt(100) surface reconstruction in electrolyte and that our results are restricted to the Pt(100)-(1 × 1) face. The potential-dependent effects of CO_{ad} interaction with the Pt-(100)-(1 × 1) surface have been investigated by measuring the scattered X-ray intensity at the first-order nonspecular CTR at 0.0 and 0.46 V in solution containing CO_b. The solid lines in Figure 5 (bottom panel) are the fits to the data which are obtained by allowing surface relaxation of the topmost Pt layer, e.g., rearrangement of atoms in which planes of atoms as a whole are displaced, but only in the direction perpendicular to the surface planes.[23] The top panel of Figure 5 shows the intensity ratio between the data sets with the solid line given by the ratio of the calculated CTR. At 0.46 V in solution saturated with CO_b, the best fit corresponds to an outward displacement of 0.04 ± 0.01 Å (or 2.2% of the bulk lattice spacing). At 0.46 V but in CO_b-free solution, the top platinum layer is expanded by only ca. 1.2%. At 0.0 V, the expansion is 0.076 Å (or 3.9% of the platinum lattice parameter), which is

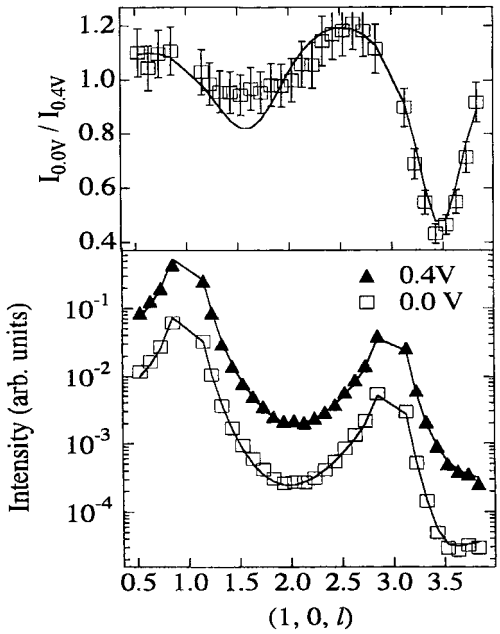

Figure 5. (Bottom panel) The first-order nonspecular CTRs for the Pt(100) surface with the electrode potential held at 0.0 and 0.4 V with a constant overpressure of CO being supplied to the X-ray outer cell. The solid lines are fits to the data. (Top panel) The intensity ratio between the data sets with the solid line given by the ratio of the calculated CTRs.

significantly greater than the 2.4% expansion observed in the presence of an adsorbed monolayer of hydrogen in CO_b-free solution.[24]

Further structural information for the Pt(100)−CO_{ad} system can be obtained by measuring the specular CTR. The specular CTR is more sensitive than the nonspecular CTR to adsorbed layers on the surface which are not commensurate with the Pt lattice, and can thus provide information on an incommensurate interlayer spacing. In Figure 6 (bottom panel), the dashed line is a calculation which includes only the effect of surface relaxation in the presence of CO_b and does not include scattering from the CO_{ad}. A close inspection of this figure reveals that the dashed line does not accurately reproduce the data, particularly at the anti-Bragg position, (0,0,3), where maximum sensitivity to adsorbed species is obtained. Good agreement with the data was obtained only when scattering from CO_{ad} is included, with a surface coverage of $\theta_{COad} = 0.8 \pm 0.5$ ML and a platinum−carbon spacing of $d_{Pt-C} = 1.4 \pm 0.4$ Å (the calculation is shown by the solid line in the bottom panel of Figure 6). The inclusion of CO_{ad} reduces the value of χ^2 for the fit from 1.9 to 0.8, so it is statistically significant. The relatively large value of χ^2 is due to the small scattering factor of CO_{ad}.

The potential dependence of the Pt(100) surface relaxation induced by the H_{upd} and/or (preadsorbed CO_{ad} at 0.05 V) is represented by the results shown in Figure 7. The surface expansion is proportional to the scattering intensity at (1,1,2.7). Surface roughness, however, reduces the intensity at (1,1,2.7). In a solution free of CO_b, in the H_{upd} region, the top platinum layer expands ca. ≈2.4% of the bulk lattice spacing away from the second layer when H_{upd} reaches a monolayer coverage at −0.05 V. Following the adsorption of CO at 0.05 V, in the same potential region (continuous flow of CO to the X-ray outer cell), the expansion is even larger, ca. 4%. After establishing the CO_{ad}-induced expansion of the Pt(100) lattice, the continuous flow of CO to the outer shell of the X-ray cell was replaced with nitrogen while holding at 0.05 V. Upon sweeping the

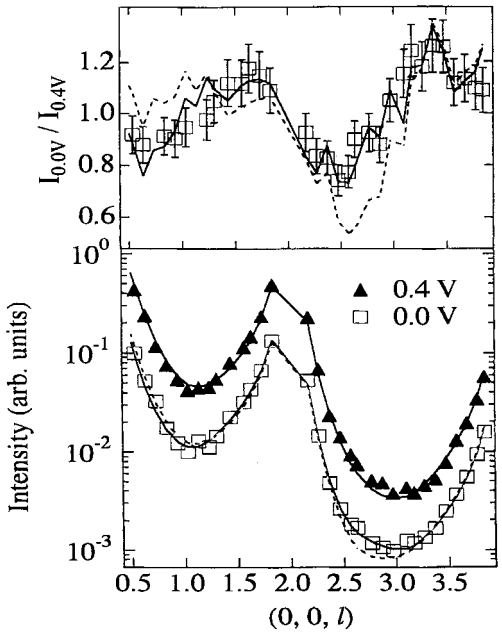

Figure 6. (Bottom panel) The first-order specular CTRs for the Pt(100) surface with the electrode potential held at 0.0 and 0.4 V in 0.5 M H_2SO_4 with a constant overpressure of CO being supplied to the X-ray outer cell. The dashed lines are the calculated CTRs which include only surface relaxation. (Top panel) The solid line is the ratio of the calculated intensities normalized to the experimental data in CO_b-saturated solution. The dashed line is the ratio of the calculated intensities normalized to the experimental data in CO_b-free solution.

potential positively from 0.05 V, the oxidation of CO_{ad}, in what we have referred to as the pre-ignition potential region (inset of Figure 1), is mirrored by a continuous contraction of the Pt surface layer, as shown in Figure 7. Above ca. 0.65 V, the top layer expansion is reduced significantly, and the measured X-ray intensity above 0.7 V drops to a value below that observed for the unrelaxed Pt(100) surface without CO_{ad}, which is different from the results observed for the Pt(111)−CO_{ad} system. This can be explained by a slight roughening of the Pt(100) surface caused by potential excursion to 0.8 V. Note there is a general decrease in intensity on the successive negative sweep, indicating some roughening.

Finally, while holding the potential at different values we have searched for ordered in-plane structures of adsorbed CO_{ad} on Pt(100). In contrast to the Pt(111)−CO_{ad} system, however, no ordered structure was observed for the Pt(100)−CO_{ad} system although the fact that CO_{ad} must be included in the modeling of the CTR intensity implies that the CO_{ad} is relatively well ordered in the surface normal direction. The fact that *no* in-plane ordered structures of CO_{ad} are observed may be due to the atomic geometry of the (100) surface where the distances between favorable CO adsorption sites frustrates the CO_{ad}−CO_{ad} interaction, i.e., the Pt−CO_{ad} band dominates the microscopic ordering of the CO_{ad} adlayer. (Note that although an order p(2 × 2)−CO_{ad} adlayer was observed on the Pt(111) surface [19], modeling of the specular CTR was not sensitive to the inclusion of a CO_{ad} adlayer.)

4. Discussion

Recent studies using the in-situ SXS technique have provided very important information about the potential-dependent structure stability of Pt(*hkl*) single-crystal surfaces, prepared by the flame-annealing method, in several CO_b-saturated electrolytes.[24−26] In contrast to UHV studies,[23] we have found that

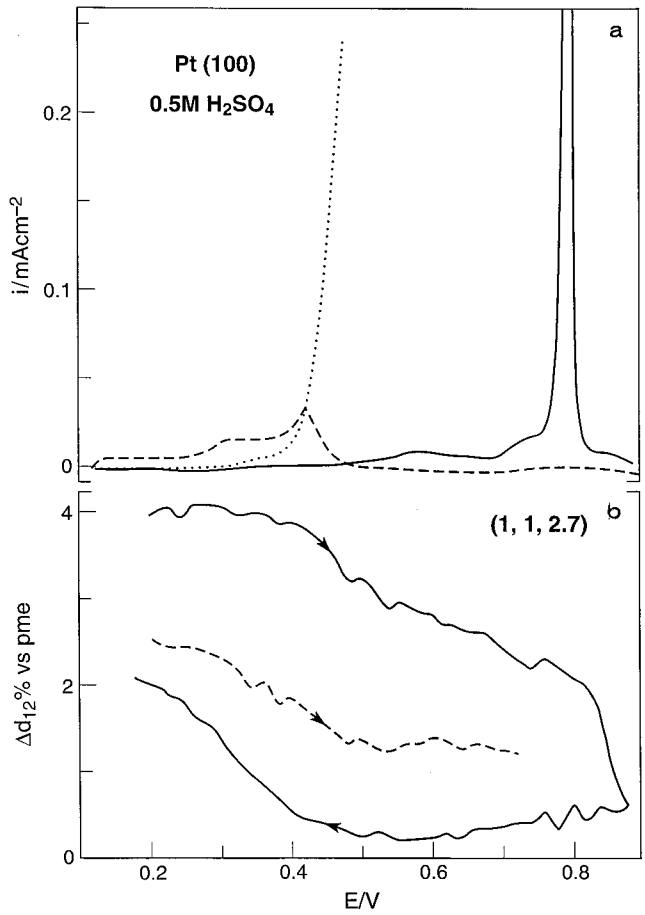

Figure 7. (—) (Bottom panel) Scattering intensity changes at measured at (1, 1, 2.7) for the Pt(100) surface in 0.5 M H_2SO_4 covered by CO_{ad} and (- - -) free of CO_{ad}; sweep rate 2mV/s. (Top panel) Stripping voltammetry of CO_{ad} is shown for comparison.

the irreversible adsorption of CO_{ad} on Pt(*hkl*) surfaces has no effect on the rearrangement of the substrate atoms to alter the surface unit cell, i.e., the surface exhibits the same structure with and without CO adsorption apart from changes in the out-of-plain relaxation of the topmost atomic layer. The electrochemical consequence of the structure stability of the Pt low-index single-crystal surfaces in solution containing CO_b is that the kinetics of CO oxidation can be examined on stable, clean, and well-oriented Pt(100)-(1 × 1), Pt(111)-(1 × 1), Pt(110)-(1 × 1), and Pt(110)-(1 × 2) surfaces.[24−26] In what follows, we compare the atomic structures of CO_{ad} layers and the kinetics of CO_{ad} oxidation on the Pt(*hkl*) surfaces that span all three low-index symmetries of the *fcc* lattice.

4.1. Displacement Effects. Electrochemical studies in this work confirmed previous findings that the formation of a close-packed monolayer of CO_{ad} on Pt(100) at 0.05 V is accompanied by complete displacement of both H_{upd} and specifically adsorbed anions (e.g., HSO_4^-, OH^-)[17,19,27]. As in the case of Pt(111) and Pt(110) surfaces, we suggest that the main forces that lead to the displacement of H_{upd} arise primarily from the strength of the adsorbate−metal bonding, the Pt(100)−CO_{ad} interaction being stronger than the Pt(100)−H_{upd} interaction. Assuming that the Gibbs energy of adsorption can be considered as a quantitative measure of the binding energy of H_{upd} and CO_{ad} at $\Theta_{ad} = 0.5$ ML, one can calculate the Gibbs energy change for the displacement process (3) from the following set of compo-

nent steps:

$$H^+ + e^- = H_{upd} \qquad \Delta G_{H_{upd}} = -nFE^{\theta=0.5}_{H_{upd}} \quad (1)$$

$$CO_b = CO_{ad} \qquad \Delta G^{\theta=0.5}_{CO_{ad}} \approx \Delta H_{ad} \quad (2)$$

$$H_{upd} + CO_b = CO_{ad} + H^+ + e^- \qquad \Delta G_d = \Delta G_{CO_{ad}} - \Delta G_{H_{upd}} \quad (3)$$

The difference in the Gibbs energy for H_{upd} adsorption[35] ($\Delta G_{H_{upd}} \approx -34 \pm 5$ kJ/mol), and for CO_{ad} on the Pt(100) surface[36] ($\Delta G_{CO_{ad}} \approx -130 \pm 15\%$ kJ/mol) corresponds to the Gibbs energy for the displacement process, $\Delta G_d \approx -96 \pm 5$ kJ/mol. In the same way we estimate that the value of ΔG_d for the other two single-crystal surfaces is also close to ca. -90 ± 5 kJ/mol.

4.2. Surface Structures at the Pt(*hkl*)−CO Interface. The analyses of SXS results in Figure 5 also confirmed our recent observation that in solution free of CO_b, where the surface is covered by a monolayer of hydrogen, the topmost Pt atomic layer was expanded, e.g., for Pt(100)−H_{upd} by ≈2.4% of the lattice spacing away from the second layer.[24] SXS results at the Pt(100)−CO_{ad} interface show that this expansion increased to ≈ 4% when H_{upd} was completely displaced by a saturated layer of CO_{ad}, see Figure 7. The difference in relaxation of the Pt(100) surface covered with H_{upd} and CO_{ad} probably arises from the difference in the adsorbate−metal bonding, the Pt(100)−CO_{ad} interaction being much stronger than the Pt(100)−H_{upd} interaction, which is in good agreement with the thermodynamic prediction.

Besides probing atomic relaxation at the Pt electrode, SXS has provided information about ordering in the adsorbate layers and the metal−adsorbate interlayer spacing. Following the adsorption of CO_{ad} on Pt(111) at 0.05 V, we observed a diffraction pattern consistent with a p(2 × 2) symmetry, $\Theta_{CO_{ad}}$ ≈ 0.75 ML. Once formed, the structure was stable even when the CO_b was replaced by nitrogen, confirming that CO_{ad} is indeed irreversibly adsorbed on the Pt surface.[19] In contrast to the Pt(111)−CO interface, no in-plane structures of CO_{ad} with long-range order were formed on either Pt(110) or Pt(100) in aqueous electrolytes. The analysis of the CTR measurements in this work, however, provided some structural information about the CO_{ad} adlayer on Pt(100). The specular CTR measurements were modeled by including a CO_{ad} layer which, at 0.05 V, gave $\Theta_{CO_{ad}} \approx 0.8 \pm 0.05$ ML and a Pt−CO surface normal interlayer spacing of 1.4 ± 0.4 Å. Assuming that CO_{ad} is covalently bonded to the platinum (the covalent radii of Pt and CO are 1.3 and 0.77, respectively[23]), the calculated values for the surface normal spacing between platinum and the CO_{ad} adsorbed on top sites, bridge sites, and 4-fold hollow sites are 2.07, 1.54, and 0.64 Å, respectively. The surface normal spacing of 1.4 ± 0.4 Å which is assessed from SXS measurements appears to rule out the possibility that CO_{ad} is adsorbed in the 4-fold hollow site, and implies that CO_{ad} occupies primarily the 2-fold bridge sites, or possibly a mixture of bridge and atop sites. This is in harmony with the Fourier transform infrared (FTIR) results for the adsorption of CO on the Pt(100) surface.[15]

4.3. Nature of CO_{ad} and Reaction Mechanism for Oxidation of CO_{ad}. Given that CO adsorption on Pt(*hkl*) at near ambient temperature is an irreversible process, it is impossible to evaluate unambiguously thermodynamic functions in aqueous electrolytes. As suggested above, in analyzing the electrochemistry of the Pt(*hkl*)-CO_{ad} system one can use the values of thermodynamic functions which are obtained from UHV measurements and test them in an electrochemical system for consistency. This process becomes somewhat more complex upon considering that the heat of adsorption of CO_{ad} on Pt(*hkl*) in UHV is coverage dependent. Nevertheless, keeping in mind that UHV values for heats of CO adsorption are relatively insensitive to the surface structure of substrate,[30] and that heats of adsorption at saturation coverage of CO_{ad} are close to ≈1/3 of the initial value,[23] using the gas-phase values we approximate a heat of adsorption of CO_{ad} at Pt(*hkl*) in sulfuric acid solution ≈150 ± 15 kJ/mol at low coverage and ≈65 ± 15 kJ/mol at saturation. For our purposes here, the exact functionality of the variation of the heat of adsorption with coverage is not of concern. Closely following our discussion for the electrooxidation of CO on Pt(111),[19] we propose that what we call a weakly adsorbed state is a high surface coverage state of CO_{ad} on Pt(*hkl*) surfaces. The weakly adsorbed state is created by the "crowding" of the surface with CO_{ad} that reduces its adsorption energy via CO_{ad}−CO_{ad} repulsion. When the coverage is reduced by oxidation, and the repulsive interaction is correspondingly reduced, the remaining CO_{ad} molecules relax into a less closely packed CO_{ad}−CO_{ad} coordination. It is this relaxed state which we characterize as the strongly adsorbed state. In keeping chemical intuition, the weakly adsorbed state is more reactive than the strongly bonded state, and thus is oxidized from the surface at a lower potential. The Pt−CO_{ad} bond energy is not, however, the only factor determining the rate of CO_b electrooxidation. This point is addressed in more detail below.

According to Figures 1 and 8, two potential regions can be resolved in both the anodic stripping voltammetry of CO_{ad} and during CO_b oxidation: a potential region of the electrooxidation of the $CO_{ad,w}$ state (the pre-ignition potential region) and the potential region of the oxidation of the $CO_{ad,s}$ state (the ignition potential region). These results reveal that while the rate of $CO_{ad,w}$ oxidation is a rather slow process, the oxidative removal of $CO_{ad,s}$ in the ignition potential region is a very fast process. Although the nature of CO_{ad} is different below and above the ignition potential we propose that the mechanism for CO_{ad} oxidation on Pt(*hkl*) is the same in both the pre-ignition and ignition potential regions, e.g., CO_{ad} reacts with OH_{ad} species through a Langmuir−Hinshelwood type reaction:[31]

$$CO_{ad} + OH_{ad} = CO_2 + H^+ + e^- \quad (4)$$

In the framework of the above discussion, the maximum rate of reaction 4 would require a half surface coverage of CO_{ad} and OH_{ad} together with a low binding energy of these species to the surface to promote rapid surface diffusion. It is important to note that in acid solutions the adsorption of OH_{ad} is also affected by specific adsorption of anions from supporting electrolytes.[32] In what follows, differences in activity of three low-index faces of Pt for CO oxidation will be discussed in the light of the structure-sensitive adsorption of OH_{ad}, CO_{ad}, and anions from supporting electrolytes.

4.3.1 Structural Effects in the Pre-Ignition Potential Region. In our earlier related studies we have found that at low potentials ($E < 0.8$ V) CO_b oxidation on Pt(110)-(1 × 1) is completely suppressed, see Figure 5 in reference 17. While the Pt(110)-(1 × 1) surface is uniquely inactive for oxidative removal of $CO_{ad,w}$ below ca. 0.8 V, the onset of $CO_{ad,w}$ oxidation on Pt(111), Pt-(110)-(1 × 2), and Pt(100) begins as early as at ca. 0.5 V, appearing as a pre-ignition peak in potentiodynamic curves. A comparison of inserts in Figures 5 and 8 in ref 17 clearly shows that in the pre-ignition potential region the rate of $CO_{ad,w}$ oxidation varies with crystal face, with activity increasing in

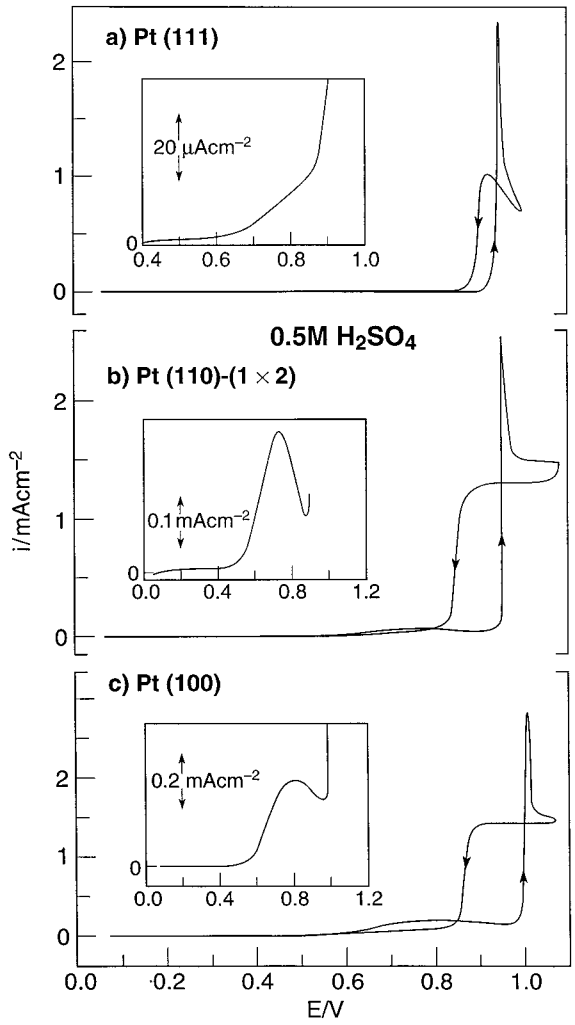

Figure 8. Potentiodynamic CO_b oxidation current densities on (a) Pt-(111)-(1 × 1), (b) Pt(110)-(1 × 2), and (c) Pt(100)-(1 × 1) in 0.5 M H_2SO_4 saturated with CO_b. Inserts: Magnification of the "pre-ignition region" from (a), (b), and (c).

the order: Pt(110)-(1 × 1)[17] ≪ Pt(111) ≪ Pt(110)-(1 × 2) ≤ Pt(100). Closely following our discussion in ref 32, it is tempting to attribute this difference in kinetics to the competitive adsorption between OH_{ad}, anions from supporting electrolytes and $CO_{ad,w}$, and subtle differences in the adsorption energies at the different crystal faces. We have suggested previously[17] that OH_{ad} and anions form selectively at defect (step) platinum sites in the pre-ignition region. Many papers have discussed the effects of surface defects in catalysis at both the solid−gas and solid−liquid interfaces. Studies of CO_{ad} oxidation in UHV have shown that the oxidative removal of CO_{ad} takes place between oxygen chemisorbed preferentially on the step sites and CO_{ad} on the terrace sites.[33] One can extend this concept to the solid−liquid interface, as such a mechanism could explain, at least in part, the structure-sensitive rate of $CO_{ad,w}$ oxidation on Pt(111), Pt(100), and the two Pt(110) surfaces. As stated above, differences in activity between these two surfaces may arise from the structure-sensitive coadsorption of CO_{ad}, OH_{ad}, and bisulfate anions. The details of the coadsorption are, however, by no means unambiguous. Nevertheless, it is essential to point out that Pt(110)-(1 × 1) exposes only first-layer atoms to reactants (CO_{ad} and OH_{ad}) and/or spectators (bisulfate anions). The formation of the CO_{ad} saturated layer on this surface can lead to a *complete* occupation of the top rows of Pt atoms by $CO_{ad,w}$, resulting in a low surface coverage by OH_{ad} and, consequently in a low rate of reaction 4. In contrast, the Pt-(110)-(1 × 2) surface may expose second- and third-layer atoms to reactants and spectators, and these species may occupy both the top rows of platinum atoms (step sites) as well as the atoms in the missing rows. Note that the missing rows in the (110)-(1 × 2) structure creates "valleys" between the (110) rows formed of three-atom-wide (111) terrace. The geometry of the adsorption sites in the valleys are like those in the "flat" (111) surface or the (111) terraces of stepped surfaces. The sites on the (110) rows of atoms are common to the step sites on many types of step−terrace structures. Thus, the (110)-(1 × 2) has the mixture of sites for coadsorption of both $CO_{ad,w}$ and OH_{ad} which are absent in the (110)-(1 × 1) structure. Considering that one can safely generalized that even "flat" low-index metal surfaces may well exhibit a certain fraction of crystallographic defects, it is reasonable to suggest that the rate of CO oxidation in the pre-ignition region on Pt(100) and Pt(111) depends on the density of mono-atomic steps capable to adsorb OH_{ad}. Recently, we suggested that the Pt(100) surface prepared by the flame annealing method is an intrinsically defected surface.[34] Therefore, the pre-ignition wave on Pt(100) can be attributed to the unique catalytic property of step/defect sites to activate adsorption of OH_{ad} species which can react with $CO_{ad,w}$ on the flat terrace sites. Based on the fact that Pt(111) surface is a less defected surface than both Pt(100) and Pt(110)-(1 × 2),[34] it is reasonable to propose that, for identical conditions, there is insufficient nucleation of OH_{ad} on Pt(111) for the oxidation of $CO_{ad,w}$ to proceed in sulfuric acid solution. Consequently, in the preoxidation region Pt(111) is less active for CO_b oxidation than either on Pt(100) or Pt(110)-(1 × 2).

4.3.2 Structural Effects at (in) the Ignition Potential Region. Further evidence of the structure effects induced by competitive adsorption of OH_{ad} with CO_{ad} and bisulfate anions was also found *at* the ignition potential and *in* the ignition potential region. It is interesting that the activity at the ignition potential increases in the opposite order compared to the pre-ignition potential region: e.g., Pt(100) < Pt(110)-(1 × 2) < Pt(111) < Pt(110)-(1 × 1). In the absence of more definitive information about the state and surface coverage by coadsorbed species, the physical model that appears to rationalize the structural sensitivity of CO_b oxidation *at* the ignition potential is one which also follows the Langmuir−Hinshelwood type surface reaction, but the rate is mainly determined by the nature of CO_{ad}. We recall that *at* the ignition potential Pt(110)-(1 × 1) and Pt(111) are highly covered by $CO_{ad,w}$ (a low rate of the oxidative removal of $CO_{ad,w}$ in the pre-ignition potential region). On the contrary, *at* the ignition potential both Pt(110)-(1 × 2) and Pt(100) surfaces are covered by the strongly adsorbed state of CO_{ad}. Given that the weakly adsorbed state is more reactive than the strongly adsorbed state of CO_{ad}, it is not surprising that *at* the ignition potential the rate of oxidation on Pt(110)-(1 × 1) and Pt(111) is much higher compared to Pt(110)-(1 × 2) and Pt-(100). *In* the ignition potential region (E > 0.95 V), however, where CO oxidation should be completely controlled by diffusion of CO_b, the variation in activity increase in a similar order as in the pre-ignition potential region: e.g., Pt(111) ≪ Pt(110)-(1 × 2) = Pt(100), see Figure 8. The variation in the rate of CO_b oxidation *in* the ignition potential region appears to be more affected by a structure-sensitive adsorption of bisulfate anions which is uniquely strong on the (111) surface. Figure 8 shows that while on Pt(110)-(1 × 2) and Pt(100) the diffusion-limited current is reached (probably when OH_{ad} is being formed on both terrace as well as step sites) a diffusion-limiting current plateau for $CO_{ad,s}$ oxidation is not observed on

the Pt(111) surface. As we have shown in our previous study of the Pt(111)−CO_{ad} system, a diffusion-limiting current plateau is observed in (sulfate-free) perchloric acid supporting electrolyte.[32] Considering that bisulfate anions are rather strongly adsorbed on Pt(111) even at high positive potentials,[19,22] we suggest that the adsorption of OH_{ad} on the (111) terrace sites is hindered by strong adsorption of bisulfate anions. This, in turn, will inhibit the kinetics of oxidative removal of CO_{ad} from the Pt(111) surface.

5. Conclusions

The Pt(100)−CO_{ad} interaction in aqueous electrolytes has been examined by using rotating disk methods in combination with in-situ surface X-ray scattering (SXS) measurements. The analyses of the SXS results have shown that the topmost platinum atoms expand away from the second layer by ca. 4% when H_{upd} was completely displaced from Pt(100) by CO to form a saturated layer of CO_{ad}. Assuming gas-phase heats of adsorption for CO_{ad} apply as well to the liquid−solid interface, we estimate that the Gibbs energy change for the displacement of H_{upd} by CO_{ad} on Pt(100) is close to −90 kJ/mol. A Pt(100)−CO_{ad} surface normal interlayer spacing of 1.4 ± 0.4 Å was extracted from SXS measurements, suggesting that CO_{ad} is adsorbed primarily at the 2-fold bridge-bonded sites, or possibly at a mixture of bridge-bonded and a-top sites. In contrast to the Pt(111)−CO_{ad} system, no structures of CO_{ad} with long-range order were formed on Pt(100).

The results presented here confirm that two different forms of CO_{ad} are formed at the Pt(100)−electrolyte interface: the weakly adsorbed state which is oxidized in the so-called preoxidation region, and the strongly adsorbed state which is only oxidized in the ignition potential region. The characterization as weakly adsorbed refers to a high-coverage state in which the adsorption energy is reduced due to the repulsive CO_{ad}−CO_{ad} interaction. We propose that oxidative removal of $CO_{ad,w}$ is accompanied by simultaneous relaxation of the CO_{ad} adlayer, and that the remaining CO_{ad} assumes a new bonding state which we term the strongly adsorbed state, $CO_{ad,s}$.

Although the nature of CO_{ad} is different in these two potential regions the mechanism for CO_{ad} oxidation on Pt(100) is the same, i.e., CO_{ad} reacts with OH_{ad} species through a Langmuir−Hinshelwood type surface reaction. In the pre-ignition region, the kinetics of oxidative removal of $CO_{ad,w}$ is controlled by the surface coverage of $OH_{ad,}$ the latter forming at low overpotentials selectively at defect (step) sites. The kinetics of CO oxidation was found to vary with crystal face. The variation in activity in the pre-ignition region increases in the order Pt(110)-(1 × 1) ≪ Pt(111) ≪ Pt(110)-(1 × 2) < Pt(100). *At* the ignition potential, however, the activity increases in the opposite order Pt(100) < Pt(110)-(1 × 2) < Pt(111) < Pt(110)-(1 × 1). Finally, *in* the ignition potential region, $E > 0.95$ V, Pt(100) and (110) are significantly more active surfaces for CO_b oxidation than Pt(111). The difference in activity is attributed to the structure-sensitive adsorption of CO, OH_{ad}, and anions from supporting electrolytes.

Acknowledgment. SXS work was carried out at the European Synchrotron Radiation Facility (ESRF), Grenoble, France, and at the Stanford Synchrotron Radiation Laboratory (SSRL). Detlef Smilgies and Nathalie Boudin are gratefully acknowledged for their support of ESRF beamline ID-10B and their contributions to the X-ray scattering experiments. This work was supported jointly by the Offices of Basic Energy Sciences, and the Office of Advanced Automotive Technologies, Electric and Hybrid Propulsion Division of the U.S. Department of Energy under Contract No. DE-AC03-76SF00098.

References and Notes

(1) Beden, B.; Bilmes, S.; Lamy, C.; Leger, J. M. *J. Electroanal. Chem.* **1983**, *149*, 295.
(2) Kitamura, F.; Takeda, M.; Takahashi, M.; Ito, M. *Chem. Phys. Lett.* **1987**, *143*, 318.
(3) Sun, S.; Clavilier, J.; Bewick, A. *J. Electroanal. Chem.* **1988**, *240*, 147.
(4) Leung, L.-W.; Wieckowski, A.; Weaver, M. J. *J. Phys. Chem.* **1988**, *92*, 6985.
(5) Zurawski, D.; Wasberg, M.; Wieckowski, A. *J. Phys. Chem.* **1988**, *94*, 2076.
(6) Feliu, J. M.; Orts, J. M.; Fernandez-Vega, A.; Aldaz, A.; Clavilier, J. *J. Electroanal. Chem.* **1990**, *296*, 191.
(7) Kinomoto, Y.; Watanabe, S.; Ito, M. *Surf. Sci.* **1991**, *242*, 538.
(8) Weaver, M. J.; Chang, S.-C.; Leung, L.-W.; Jiang, X.; Rubel, M.; Szklarczyk, M.; Zurawski, D.; Wieckowski, A. *J. Electroanal. Chem.* **1992**, *327*, 247.
(9) Clavilier, J.; Albalt, R.; Gomez, R.; Feliu, J. M.; Aldaz, A. *J. Electroanal. Chem.* **1992**, *330*, 489.
(10) Orts, J. M.; Fernandez-Vega, A.; Feliu, J. M.; Aldaz, A.; Clavilier, J. *J. Electroanal. Chem.* **1992**, *327*, 191.
(11) Kita, H.; Narumi, H.; Ye, S.; Naohara, H. *J. Appl. Electrochem.* **1993**, *23*, 589.
(12) Villegas, I.; Weaver, M. J. *J. Chem. Phys.* **1994**, *101*, 1648.
(13) Couto, A.; Perez, M.; Rincon, A.; Gutierrez, C. *J. Phys. Chem.* **1996**, *100*, 19538.
(14) Wieckowski, A.; Rubel, M.; Gutierrez, C. *J. Electroanal. Chem.* **1995**, *382*, 97.
(15) Kita, H.; Naohara, H.; Nakato, T.; Taguchi, S.; Aramata, A. *J. Electroanal. Chem.* **1995**, *386*, 197.
(16) Hayden, B. E.; Murray, A. J.; Parsons, R.; Pegg, D. J. *J. Electroanal. Chem.* **1996**, *409*, 51.
(17) Marković, N. M.; Grgur, B. N.; Lucas, C. A.; Ross, P. N. *Surf. Sci.* **1997**, *384*, L 805.
(18) Gomez, R.; Feliu, J. M.; Aldaz, A.; Weaver, M. J. *Surf. Sci.* **1998**, *410*, 48.
(19) (a) Marković, N. M.; Grgur, B. N.; Lucas, C. A.; Ross, P. N. *J. Phys. Chem. B* **1999**, *103*, 487. (b) Lucas, C. A.; Marković, N. M.; Ross, P. N. *Surf. Sci.* **1999**, *425*, L 381.
(20) Marković, N. M.; Gasteiger, H. A.; Ross, P. N. *J. Phys. Chem.* **1995**, *99*, 3411.
(21) Lucas, C. A.; Marković, N. M.; Ross, P. N. *Phys. Review B* **1998**, *57*, 13184.
(22) Marković, N. M.; Marinković, N. S.; Aldaz, R. R. *J. Electroanal. Chem.* **1988**, *214*, 309.
(23) Somorjai, G. A. In *Introduction to Surfce Chemistry and Catalysis*; John Wiley & Sons Inc., New York, 1994.
(24) Tidswell, I. M.; Marković, N. M.; Ross, P. N. *Phys. Rev. Letter* **1993**, *71*, 1601.
(25) Tidswell, I. M.; Marković, N. M.; Ross, P. N. *J. Electroanal. Chem.* **1994**, *376*, 119.
(26) Lucas, C. A.; Marković, N. M.; Ross, P. N. *Phys. Rev. Letter* **1996**, *77*, 4922.
(27) Orts, J. M.; Gomez, R.; Feliu, J. M.; Aldaz, A.; Clavilier, J. *J. Electrochim. Acta.* **1995**, *39*, 1519.
(28) Marković, N. M.; Grgur, B. N.; Ross, P. N. *J. Phys. Chem.* **1997**, *101*, 5405.
(29) Thiel, P. A.; Behm, R. A.; Norton, P. R.; Ertl, G. *J. Chem. Phys.* **1983**, *78*, 7458.
(30) Lee, W. T.; Ford, L.; Blowers, P.; Nigg, H. L.; Masel, R. I. *Surf. Sci.* **1998**, *416*, 141.
(31) Ertl, G. In *Chemistry and Physics of Chemical Surfaces*, Vol. 2; Vanselow, R., England, W., Eds.; CRC Press Inc., Boca Raton, FL, 1982, pp 21−28.
(32) Marković, N. M.; Schmidt, T. J.; Grgur, B. N.; Gasteiger, H. A.; Behm, R. J.; Ross, P. N. *J. Phys. Chem.*, accepted.
(33) Xu, J.; Yates, J. T. *J. Chem. Phys.* **1993**, *99*, 725.
(34) (a) Lucas, C. A.; Marković, N. M.; Ross, P. N. *Langmuir* **1997**, *44*, 1009. (b) Marković, N. M.; Grgur, B. N.; Lucas, C. A.; Ross, P. N. *Electroch. Acta* **1998**, *13*, 5520.
(35) Unfortunately, because of close coupling of specific adsorption of bisulfate anions with H_{upd}, the thermodynamic functions for the H_{upd} state on Pt(100) cannot be unambiguously estimated from the adsorption isotherm of H_{upd}.[28] The best estimate of the Gibbs energy for H_{upd} on Pt(100) may be obtained from the underpotential shift $\Delta Ep \approx 0.36$ V corresponding to $\theta_{Hupd} = 0.5$ ML referred to the potential of the $1/2H_2/H^+$ electrode in the same solution at the same temperature.
(36) Assuming that a heat of adsorption of CO_{ad} at the Pt(*hkl*)−gas interface is the best approximation for a heat of adsorption at the Pt(*hkl*)−liquid interface, we estimate $\Delta G_{CO_{ad}}^{\theta=0.5}$ at the Pt(100-(1 × 1)−CO_{ad} liquid interface to be ≈135 ± 15 kJ/mol, which is equal to $\Delta G_{CO_{ad}}^{\theta=0.5}$ determined for the Pt(100)-(1 × 1)−CO_{ad} gas interface.[29]